

Supersymmetric Heavy Higgs Bosons at the LHC

Alexandre Arbey*

*Centre de Recherche Astrophysique de Lyon, Observatoire de Lyon,
Saint-Genis Laval Cedex, F-69561, France; CNRS, UMR 5574;
Ecole Normale Supérieure de Lyon, France;
Université de Lyon, Université Lyon 1, F-69622 Villeurbanne Cedex, France
and CERN Theory Division, CH-1211 Geneva, Switzerland*

Marco Battaglia†

*University of California at Santa Cruz,
Santa Cruz Institute of Particle Physics, CA 94720, USA
and CERN, CH-1211 Geneva, Switzerland*

Farvah Mahmoudi‡

*Clermont Université, Université Blaise Pascal, CNRS/IN2P3,
LPC, BP 10448, F-63000 Clermont-Ferrand, France
and CERN Theory Division, CH-1211 Geneva, Switzerland*

The search for heavy Higgs bosons is an essential step in the exploration of the Higgs sector and in probing the Supersymmetric parameter space. This paper discusses the constraints on the M_A and $\tan\beta$ parameters derived from the bounds on the different decay channels of the neutral H and A bosons accessible at the LHC, in the framework of the phenomenological MSSM. The implications from the present LHC results and the expected sensitivity of the 14 TeV data are discussed in terms of the coverage of the $[M_A - \tan\beta]$ plane. New channels becoming important at 13 and 14 TeV for low values of $\tan\beta$ are characterised in terms of their kinematics and the reconstruction strategies. The effect of QCD systematics, SUSY loop effects and decays into pairs of SUSY particles on these constraints are discussed in details.

PACS numbers: 12.60.Jv, 14.80.Da

I. INTRODUCTION

With the observation of a light Higgs-like particle by the ATLAS and CMS experiments at the LHC [1, 2], the detailed exploration of the Higgs sector becomes one of the most compelling programs of collider physics. In particular, understanding whether this sector extends beyond that of the Standard Model (SM) and heavier Higgs bosons exist is of crucial importance for the viability of several models of new physics beyond the Standard Model, *in primis* of Supersymmetry (SUSY). This question can be answered either through a precision study of the couplings of the lightest boson, h , or by direct searches of the additional, heavier states which characterise extended Higgs models.

The LHC experiments have not only observed a light state and obtained the first determination of its decay rates to $\gamma\gamma$, WW and ZZ . They have also performed

several searches directly probing the possible production of heavy Higgs bosons and other searches, which can now be re-interpreted in order to set constraints on the production and decays of neutral heavy Higgs states. However, these data are still largely fragmentary.

Several studies of the MSSM heavy Higgs sector at LHC results have already been performed [3–7]. This paper intends to provide a comprehensive assessment of the present status and the future perspectives for the constraints on the MSSM Higgs sector parameters, from the identification of the main processes relevant to the LHC searches to a systematic study of the exclusion limits derived from the combination of the LHC results, in the context of the phenomenological MSSM (pMSSM) with the neutralino as the lightest SUSY particle (LSP) [8]. We perform this study taking the mass of the heavy pseudoscalar, M_A , and the ratio of the vacuum expectation value of the two Higgs doublets, $\tan\beta$, as the main parameters. We highlight the complex pattern of decays arising at low values of $\tan\beta$, values which are shown to be compatible with the present data and discuss the complementarity of decay modes such as $H \rightarrow ZZ$, tt and hh and $A \rightarrow Zh$.

The combination of the relevant decay channels to ex-

*Electronic address: alexandre.arbey@ens-lyon.fr

†Electronic address: MBattaglia@lbl.gov

‡Electronic address: mahmoudi@in2p3.fr

tend the sensitivity of the heavy Higgs searches over most of the $[M_A - \tan\beta]$ was already discussed in [9]. Here, we use the published and preliminary results for the expected upper limits on the product of production cross section and decay branching fraction in several channels as constraints and extrapolate them to the full 2012 data set of 25 fb^{-1} /experiment at 8 TeV and to 150 fb^{-1} of 14 TeV data.

In section II, we discuss the production and decays of the H and A neutral bosons, with special emphasis for the low $\tan\beta$ region. Section III is devoted to presentation of the results of our systematic study of the indirect constraints derived from the latest measurements of the decay rates of the 126 GeV Higgs-like particle together with those obtained from direct searches for $H/A \rightarrow \tau^+\tau^-$, $H_{SM} \rightarrow ZZ$, $bbH \rightarrow bbbb$ and resonant tt production and their expected sensitivity on the 14 TeV LHC data. Then, we review additional decay modes, which have not yet been considered in the LHC searches but will become important at 14 TeV in the low $\tan\beta$ region and characterise their kinematics and reconstruction strategies. Finally, we discuss the validity of these bounds when taking into account the production cross section uncertainties and the role of SUSY particles affecting the decays of heavy Higgs bosons, either in their direct decays to SUSY states or through loop corrections to their decay widths. Section IV has the conclusions.

II. THE HIGGS SECTOR AND THE $M_A - \tan\beta$ PARAMETERS

A. H and A production and decays in the pMSSM

The MSSM neutral heavy Higgs bosons H and A have couplings modified compared to the SM Higgs state. In the decoupling limit ($M_A \gg M_Z$), the H/A coupling to the top quarks is suppressed by $1/\tan\beta$, while the couplings to bottom quarks and tau leptons are enhanced by $\tan\beta$. As a consequence, the H/Att coupling is important only for $\tan\beta \lesssim 10$, those to bb and $\tau\tau$ becoming dominant for larger values. On the other hand, the H couplings to vector bosons are suppressed by a factor $\cos(\beta - \alpha)$, which in the large M_A and $\tan\beta$ limit, decreases as $1/\tan\beta$. The situation is the same for the AhZ coupling, while there is no A coupling to vector bosons at tree level. Finally, the coupling of the H to hh also decreases in the large M_A and $\tan\beta$ limit with $1/\tan\beta$. Hence, the description of the heavy Higgs sector in the large $\tan\beta$ limit is simply dominated by the couplings to b and τ fermions, whereas in the small $\tan\beta$ regime, a rich phenomenology emerges, as the other couplings become important. A thorough discussion can be found in Ref. [10].

The H and A production cross section is dominated by the gluon fusion process and the associate Higgs production with b quarks. The relevant cross sections are shown in Fig. 1 for two values of the pseudoscalar Higgs

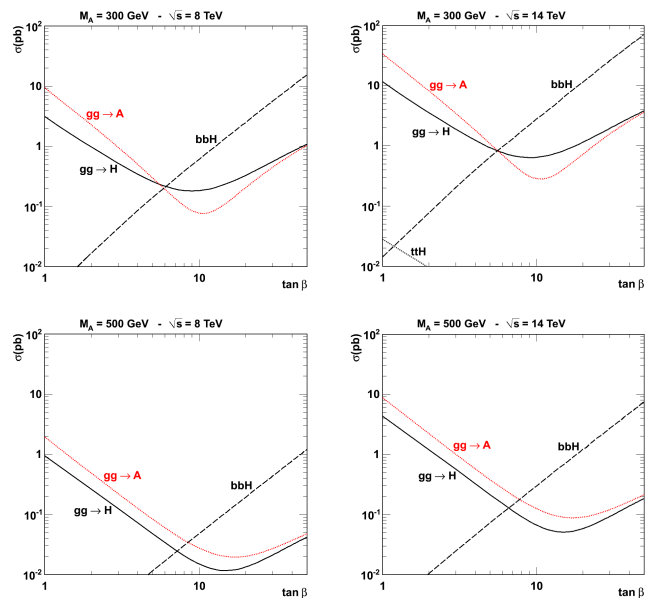


FIG. 1: Production cross sections for H and A bosons as a function of $\tan\beta$ in pp collisions at 8 TeV (right panels) and 14 TeV (left panels) for $M_A = 300$ GeV (upper panels) and 500 GeV (lower panels).

mass ($M_A = 300$ and 500 GeV) at $\sqrt{s} = 8$ and 14 TeV, as a function of $\tan\beta$.

The bbH associate production is a tree level process, which increases as $\tan^2\beta$ and becomes dominant for $\tan\beta \gtrsim 10$. Instead, the gluon fusion processes [11], induced by top and bottom quark loops, have the top loops dominant at small $\tan\beta$, resulting in a decrease of the total cross section with $\tan\beta$ up to the point where the b loops take over and the total cross section increases. Finally, the ttH production mode is kinematically suppressed and decreases with $1/\tan^2\beta$, while vector boson fusion and associate production with gauge bosons is not important, contrary to the case for the lightest Higgs boson.

The decay $A/H \rightarrow \tau^+\tau^-$ is the main process for the LHC experiments to search for the neutral heavy Higgs bosons at the present LHC energy, the dominant decay into $b\bar{b}$ being overwhelmed by the SM multi-jet background. As such, the $\tau\tau$ mode has so far attracted most of the attention in the LHC searches for heavy Higgs bosons. At intermediate to large values of $\tan\beta$ the $\tau\tau$ and bb channels saturate the decay widths of the A and H . At low $\tan\beta$ the decay pattern of the heavier MSSM Higgs particles becomes more complicated by the onset of several decay modes which compete with $\tau\tau$, in particular WW , ZZ , tt and hh . The branching fractions for the decays of H and A bosons are shown in Fig. 2 as a function of $\tan\beta$ for two masses below (300 GeV) and above (500 GeV) the $t\bar{t}$ threshold.

The main features can be summarised as follows. Below the tt threshold, the H boson decays into gauge bosons $H \rightarrow WW, ZZ$ and into pairs of the light

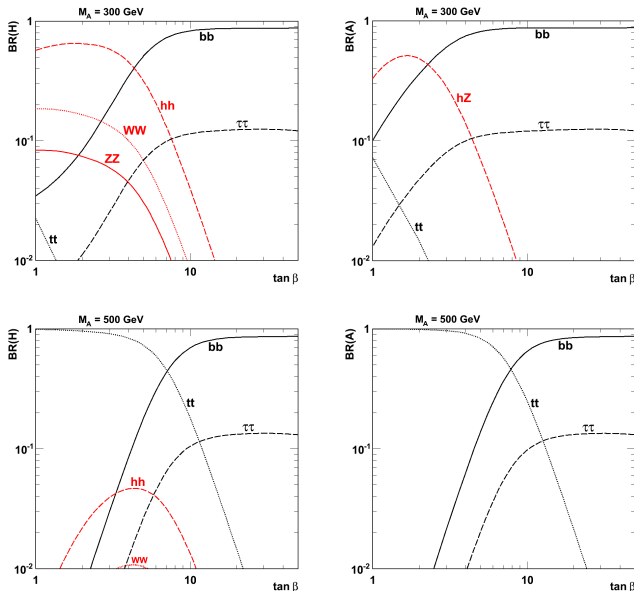


FIG. 2: Decay branching fractions for H (left) and A (right) bosons of mass 300 GeV (above) and 500 GeV (below) as a function of $\tan\beta$, in absence of decay channels into SUSY particles.

Higgs boson, hh have substantial rates. In the interval $2M_h \lesssim M_H \lesssim 2m_t$, this interesting channel, $H \rightarrow hh$, becomes the dominant decay mode for $\tan\beta \sim 3$. Similarly the pseudoscalar A boson decays into hZ with a significant rate, above threshold and at low $\tan\beta$. For heavier H/A masses, the top decay channels, $H, A \rightarrow t\bar{t}$, becomes dominant below $\tan\beta \sim 5 - 10$.

Figure 3 shows the regions in the $[M_A - \tan\beta]$ plane of the pMSSM parameter space, where the branching fractions of $H \rightarrow ZZ/WW$, $H/A \rightarrow t\bar{t}$ and $H \rightarrow hh$ are larger than 1%, 5% and 10%. As can be seen, $\text{BR}(H/A \rightarrow ZZ/WW, hh)$ can be large in the small to intermediate $\tan\beta$ and M_A region. Above the threshold, the $\text{BR}(H \rightarrow t\bar{t})$ is large for $\tan\beta \lesssim 20$ independently of the M_A value.

The exclusion limits in the $[M_A - \tan\beta]$ plane may be modified when some light SUSY particles are present in the spectrum. In particular, three scenarios can affect the $[M_A - \tan\beta]$ bounds. First, light SUSY particles, with masses $\lesssim \frac{1}{2}M_{H/A}$ may induce SUSY decays of the H/A states thus reducing the $H/A \rightarrow \tau^+\tau^-$ branching fraction. For $M_A \lesssim 1$ TeV, these SUSY particles can be light neutralinos or charginos, indicated collectively with $\tilde{\chi}$ in the following, and light sleptons, in particular staus, $\tilde{\tau}$, in the case of the CP-even H boson while for the pseudoscalar A , only decays $A \rightarrow \tilde{\tau}_1\tilde{\tau}_2$ are allowed.

The pMSSM, due to the uncorrelated mass values of the SUSY particles afforded by its 19 free parameters, offers a convenient framework for this study, in particular by revealing scenarios where decays into SUSY particles may be important. The scans used for this study with the constraints and the relevant ranges for the variation of the pMSSM parameters have been already presented in

Ref. [12, 13]. In this analysis, we start from a large sample of 2×10^8 generated pMSSM points and select those fulfilling the constraints from LEP data, flavour physics, dark matter and \tilde{g}, \tilde{q} direct searches at LHC as discussed in Ref. [12]. In particular, we apply the constraints derived from the rare decay $B_s \rightarrow \mu\mu$ and direct dark matter searches, also providing us with constraints to the $[M_A - \tan\beta]$ parameter space [14, 15], and we impose that one of the neutral Higgs bosons has a mass in the range 121.5 to 129.9 GeV to be consistent with the results of the SM Higgs searches, as discussed below.

The LHCb experiment has recently announced the first evidence for the $B_s \rightarrow \mu^+\mu^-$ decay and measured its branching fraction to be in agreement with the SM expectation [16]. This branching ratio is sensitive to the Higgs sector, in particular to M_A and $\tan\beta$, proportional to $\sim \tan^6\beta/M_A^4$ in the large $\tan\beta$ limit. Complementary information is also obtained by dark matter direct detection experiments, in particular the latest XENON-100 limits [17], probing the scattering of neutralino with matter, which can be mediated by scalar particles.

The tools used to perform the scans and the analysis have been presented in Ref. [14, 18]. Most relevant to this study are the calculations of the Higgs decay branching fractions and production cross sections. The first are computed using the latest version of HDECAY (5.10) [19]. The cross section for $gg \rightarrow H/A$ process is computed at NNLO with HIGLU 3.1 [20, 21], that for $bb \rightarrow H/A$ at NNLO with bbb@nnlo [22] and that for $pp \rightarrow bbH$ at LO with HQQ [23]. In addition, we compare the results for gg and $bb \rightarrow H/A$ from these programs to those from SusHi [24] and found an agreement within 10-15%. The Higgs and superparticle spectra are calculated with Softsusy 3.2.3 [25] and SuperIso Relic v3.2 [26, 27] computing the dark matter relic density and flavour constraints and providing the central control program interfaced to the other codes.

B. SUSY Effects in H and A Decays

There are regions of the MSSM parameter space where the $\tau\tau$ channel is suppressed and the limits derived in this channel are correspondingly relaxed. These may be due to direct decays of H/A to SUSY particles or to loop corrections to the H/Abb vertices, affecting the $H/A \rightarrow \tau\tau$ branching fraction.

We consider first the decays of heavy neutral Higgs bosons into pairs of SUSY particles. The heavy Higgs bosons couple to charginos and neutralinos, primarily to identical particles for the mixed gaugino/higgsino states, and to different particles in case of pure gaugino or higgsino states. If the decay to charginos is allowed, it dominates over the decays to neutralinos. Heavy neutral Higgs bosons also couple to scalar fermions. However, decays to scalar fermions of the first two generations are suppressed and only significant at low $\tan\beta$, where they are sub-dominant. For scalar fermions of the third genera-

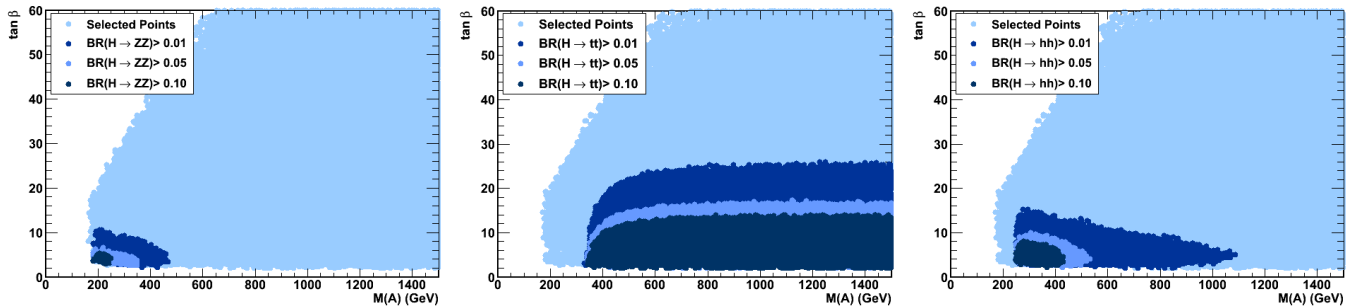


FIG. 3: Branching fraction for $H \rightarrow ZZ$ (left), $\rightarrow t\bar{t}$ (centre) and $\rightarrow hh$ (right) for the selected pMSSM points in the $[M_A - \tan\beta]$ plane.

tion the decay rates can be much larger, but they are suppressed at large $\tan\beta$ for scalar top quarks, while they are enhanced for the scalar taus and scalar bottoms. Since the lightest scalar tau, $\tilde{\tau}_1$ is often the NLSP at large $\tan\beta$, decays to staus are usually the dominant channel for decays into scalar fermions.

Figure 4 shows the decay branching fraction of H into any pair of SUSY particles calculated for the accepted pMSSM points for which at least one of these decay channels is kinematically allowed. In approximately 25% of these cases the branching fraction into SUSY particles is larger than 0.10.

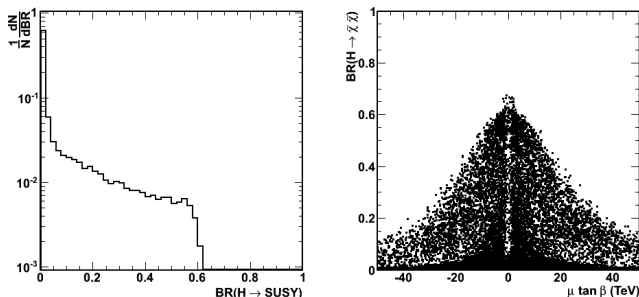


FIG. 4: Decay branching fractions for H into SUSY particles. In the left panel branching fraction for inclusive decays into any pairs of SUSY particles for the accepted pMSSM points where at least one of these decay channels is kinematically allowed. In the right panel, branching fraction into pairs of charginos and neutralinos, $\tilde{\chi}\tilde{\chi}$ as a function of $\mu \tan\beta$.

The yield in the $\tilde{\chi}\tilde{\chi}$ channels, representing the sum of all the kinematically accessible chargino and neutralino pairs, depends on the mass parameter M_2 and the Higgsino mass mixing parameter μ . Figure 5 shows the $\sigma \times \text{BR}$ product in the $[\mu - M_2]$ parameter plane to highlight the enhancement of this class of decays along the small M_2 or μ regions.

The rates of decays into SUSY particles depend mostly on the difference between the masses of heavy boson and those of the SUSY particles. As the scale of the mass of the H and A bosons probed at the LHC increases, decays into SUSY particles become more likely and have to be carefully considered. The relevant mass patterns are

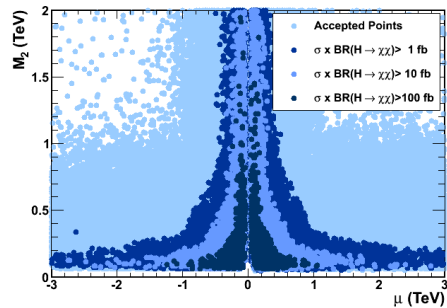


FIG. 5: Product of production cross section and decay branching fraction for $H \rightarrow \tilde{\chi}\tilde{\chi}$ at 14 TeV in the $[\mu - M_2]$ parameter plane. The dots in the light colour show all the selected pMSSM points and those in darker shades of colour the points having $\sigma \times \text{BR}$ larger than 1, 10 and 100 fb.

extensively probed in our pMSSM scans. The increase in the branching fractions of any of these SUSY channels is correlated to the decrease of that for the $\tau\tau$ mode, which can be suppressed by a factor of two, or more, compared to its average value at large M_A and $\tan\beta$ values.

Finally loop corrections to the Hbb and $A\bar{b}b$ vertices, known as Δ_b corrections [28], modify both the H/A production rates and their decay widths. In the decoupling limit, the H/A coupling to $b\bar{b}$ is modified by a factor $(1 + \Delta_b)^{-1}$, where

$$\Delta_b \approx \frac{2\alpha_s}{3\pi} \mu M_3 \frac{\tan\beta}{\max(M_3^2, m_{\tilde{b}_1}^2, m_{\tilde{b}_2}^2)} + \frac{\mu A_t}{16\pi^2} \frac{y_t^2 \tan\beta}{\max(\mu^2, m_{\tilde{t}_1}^2, m_{\tilde{t}_2}^2)}. \quad (1)$$

Full one loop corrections to the WW and ZZ decays have also been computed [29, 30]. We observe that the $\text{BR}(H/A \rightarrow \tau\tau)$ is reduced as a result of the enhancement of $\text{BR}(H/A \rightarrow b\bar{b})$ due to these corrections for SUSY parameters yielding a large Δ_b of negative sign (see Figure 6). Such a large, negative Δ_b term has also implications on the decay branching fractions of the lightest h boson. In the region where the $H \rightarrow \tau\tau$ decay rate is reduced, the branching fraction $\text{BR}(h \rightarrow b\bar{b})$ is also reduced and those for the other modes correspondingly increased.

These patterns might be tested through more precise determinations of the signal strengths of the lightest Higgs decays. In view of these effects, redundancy obtained through search in multiple channels sensitive in the same regions of the $[M_A - \tan\beta]$ parameter space appears to be essential.

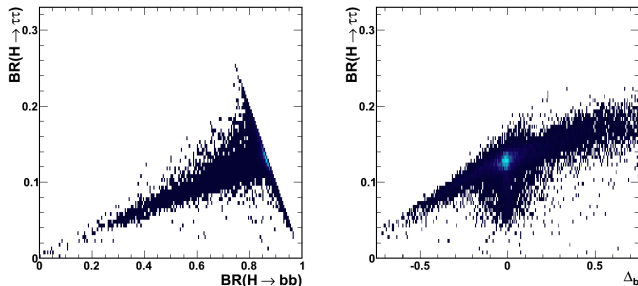


FIG. 6: Correlation of the $\text{BR}(H \rightarrow \tau\tau)$ with $\text{BR}(H \rightarrow b\bar{b})$ (left) and with Δ_b (right) for accepted pMSSM points. The correlated suppression of both the $\tau\tau$ and $b\bar{b}$ branching fractions are due to additional decays into SUSY particles, while the decrease of $\tau\tau$ with the increase of $b\bar{b}$ is due to Δ_b effect.

C. Constraints from the h Mass and Decay Rates

Assuming that the observed ~ 126 GeV state is the lightest Higgs boson of the MSSM, h , its mass M_h depends on several SUSY parameters, in particular M_A , $\tan\beta$ and the SUSY scale, $M_S = \sqrt{m_{t_1} m_{t_2}}$. The LEP-2

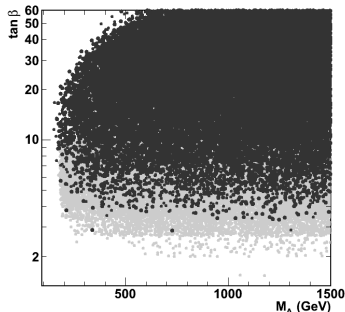


FIG. 7: The $[M_A - \tan\beta]$ parameter space compatible with $121.5 < M_h < 129.9$ GeV for different SUSY scales M_S . Distribution of the accepted pMSSM points in the $[M_A - \tan\beta]$ compatible with the M_h mass interval for $0.5 < M_S < 3.5$ TeV (black dots) and $5 < M_S < 20$ TeV (light grey dots).

limit [31], $M_h > 114.5$ GeV has been long used to define a constraint in the $[M_A - \tan\beta]$ plane, corresponding to $\tan\beta \gtrsim 2.4$ for $M_S = 1$ TeV and $M_{\text{top}} = 172.9$ GeV [32] in the so-called M_h^{max} scenario [33]. Now, each value of M_h defines a constraint in the $[M_A - \tan\beta]$ which depends on M_S . A larger value of M_S corresponds to a weaker constraint on $\tan\beta$. Therefore, it is possible to set a large enough M_S scale which recovers the low $\tan\beta$ solutions of the MSSM, even by applying the LHC constraints for

M_h , which are now significantly stronger than the LEP-2 limit. This is illustrated in Figure 7 which shows the values of $\tan\beta$ vs. M_A for our pMSSM scans which are compatible with $121.5 < M_h < 129.9$ GeV, for two intervals of values of the SUSY scale M_S . Large enough M_S values rescue the MSSM scenarios at low values of $\tan\beta$, provided we accept a high fine tuning parameter from the large scale of M_S . This observation motivates the special attention we have chosen to devote to low $\tan\beta$ scenarios in this study.

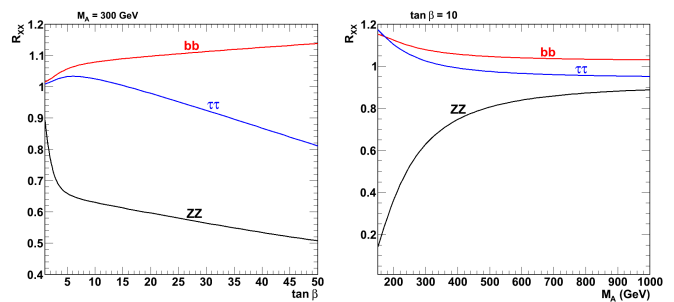


FIG. 8: Scaling of the h branching fractions into $b\bar{b}$, $\tau\tau$ and ZZ normalised to their SM value as a function of $\tan\beta$ for $M_A = 300$ GeV (left panel) and as a function of M_A for $\tan\beta = 10$ (right panel).

A second set of indirect constraints is derived by the measured h decay rates. For large M_A values, the couplings of the h boson can be expanded in powers of M_Z/M_A to obtain the following tree-level result [10]:

$$g_{hVV} \xrightarrow{M_A \gg M_Z} 1 - \frac{M_Z^4}{8M_A^4} \sin^2 4\beta \xrightarrow{\tan\beta \gg 1} 1 - \frac{2M_Z^4}{M_A^4 \tan^2 \beta} \quad (2)$$

For $M_A \gg M_Z$, g_{hVV} reaches the SM value, more quickly if $\tan\beta$ is large. The h couplings to up- and down-type fermions scale as [10]:

$$g_{huu} \xrightarrow{M_A \gg M_Z} 1 + \frac{M_Z^2}{2M_A^2} \frac{\sin 4\beta}{\tan \beta} \xrightarrow{\tan\beta \gg 1} 1 - \frac{2M_Z^2}{M_A^2 \tan^2 \beta} \quad (3)$$

$$g_{hdd} \xrightarrow{M_A \gg M_Z} 1 - \frac{M_Z^2}{2M_A^2} \sin 4\beta \tan \beta \xrightarrow{\tan\beta \gg 1} 1 + \frac{2M_Z^2}{M_A^2} \quad (4)$$

The couplings of the h boson approach those of the SM Higgs boson for $M_A \gg M_Z$ and these limits are reached at lower values of M_A for large $\tan\beta$ (see Figure 8). In practice, the ratio of branching fractions $R_{XX} = \text{BR}(h \rightarrow XX)/\text{BR}(H_{\text{SM}} \rightarrow XX)$ or the signal strengths $\mu_{XX} = \sigma(h)/\sigma(H_{\text{SM}}) \times R_{XX}$, where σ is the relevant production cross section, can be used to set constraints on the value of M_A . The recent approximate N³LO calculation of the Higgs production cross section resulting in a 17% correction also needs to be taken into account [34]. The latest set of LHC results already allows us to evaluate some non-trivial constraints, as discussed in the next section.

III. CONSTRAINTS IN THE $M_A - \tan\beta$ PLANE

The LHC searches have gathered a significant corpus of results, which can be used to place some important constraints on the H and A bosons in a variety of channels. These results also allow us to study the expected sensitivity of data to be taken at 13 and 14 TeV from 2015. In the next two sections we discuss the current constraints and in the following we present the extrapolation to 14 TeV. There are important decay channels, such as $H/A \rightarrow hh$ and $A \rightarrow hZ$, for which no analysis has been performed yet on the LHC data. We characterise the kinematics and reconstruction strategy for these processes using parametrised simulation at the end of this section.

A. Present Constraints (7 and 8 TeV)

1. Indirect Constraints from the light Higgs signal

The ATLAS and CMS collaboration have recently updated their determination of the mass and signal strengths of the Higgs-like particle. In particular, results for the $\gamma\gamma$ [35, 36], ZZ [37, 38] and WW [39, 40] channels have been reported by both collaborations for the full 8 TeV data set, corresponding to integrated luminosities of up to 25 fb^{-1} . In addition, CMS has updated the search in the $\tau\tau$ channel at low mass [41]. Here we use the weighted averages for the mass and signal strengths in these preliminary results, as summarised in Table I. For the important $\gamma\gamma$ channel we average the preliminary results of the multi-variate and cut-based analyses of CMS accounting for the quoted correlation [48]. The results of the two collaborations are only marginally consistent and we therefore rescale the error of the combined result according to the prescriptions of the Particle Data Group [42]. We use these new inputs and perform an analysis of the regions of MSSM parameter space favoured by these data. The analysis follows the strategy discussed in [13]. We define the 90% C.L. region corresponding to observables given in Table I by constructing the corresponding χ^2 probability. We account for the theory uncertainties on the MSSM h mass, $\pm 1.5 \text{ GeV}$, and the Higgs production rates, $\pm 20\%$. No signal evidence has been reported for the $b\bar{b}$, where we also include the combined estimate on μ_{bb} obtained by CDF and D0 at the Tevatron [45], and the $\tau^+\tau^-$ channels. For these we add the contribution to the total χ^2 only when the respective μ value is outside the $\pm 1.5 \sigma$ interval from the measured central value. Compared to the results available at the end of 2012, we register a marked realignment of the average values for the μ_{XX} signal strengths from the ATLAS and CMS results around the SM values. This has important consequences on the constraints derived. In particular, the M_A bound derived from the new data is about 100 GeV lower compared to that obtained on the first preliminary results on part of the 8 TeV data re-

leased at the end of 2012, without the CMS re-analysis of the $\gamma\gamma$ channel [13]. This clearly shows that it is difficult to predict the sensitivity achievable in future for these indirect limits, which depends not only on the accuracy of the inputs but also rather critically on the measured values.

Parameter	Value	Experiment
M_h (GeV)	125.7 ± 0.4	ATLAS[46]+CMS[38]
$\mu_{\gamma\gamma}$	1.20 ± 0.30	ATLAS[35]+CMS[36]
μ_{ZZ}	1.10 ± 0.22	ATLAS[37]+CMS[38]
μ_{WW}	0.77 ± 0.21	ATLAS[39]+CMS[40]
$\mu_{b\bar{b}}$	1.12 ± 0.45	ATLAS[43]+CMS[44]+(CDF+D0)[45]
$\mu_{\tau\tau}$	1.01 ± 0.36	ATLAS[47]+CMS[41]

TABLE I: Input values for the average values of the h mass and signal strengths used for this study with their statistical accuracies. Systematic uncertainties are discussed in the text.

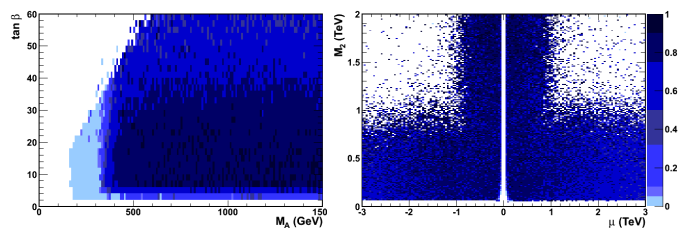


FIG. 9: Fractions of pMSSM points compatible at 90% C.L. with the constraints of Table I in the $[M_A - \tan\beta]$ (left) and $[\mu - M_2]$ (right).

We consider points compatible at 90% C.L. with these inputs accounting for theory uncertainties. We observe that these account for 76% of the accepted pMSSM points, up from the 30% obtained in the same analysis performed on the earlier data. For all these points the $\sim 126 \text{ GeV}$ state observed by ATLAS and CMS is the lightest Higgs, h . Therefore we confirm the results from our previous analysis where we did not find any pMSSM solution compatible with the LHC Higgs results where the 126 GeV particle is either the H or the A boson. This result provides an answer to the question of [49]. Figure 9 shows this fraction as a function of $[M_A - \tan\beta]$ and $[\mu - M_2]$. From the $[M_A - \tan\beta]$ distribution of these points we define the region containing 99% of the points compatible at 90% C.L. with the LHC Higgs results. This region defines an indirect lower bound on M_A , which will be compared to the direct exclusion from H/A searches in the next section.

2. Direct Constraints from MSSM Higgs Searches

Searches for the $H/A \rightarrow \tau^+\tau^-$ process have been conducted by the ATLAS with 4.7 fb^{-1} at 7 TeV [50] and CMS with $4.8+12.2 \text{ fb}^{-1}$ at 7 and 8 TeV [51]. The CMS

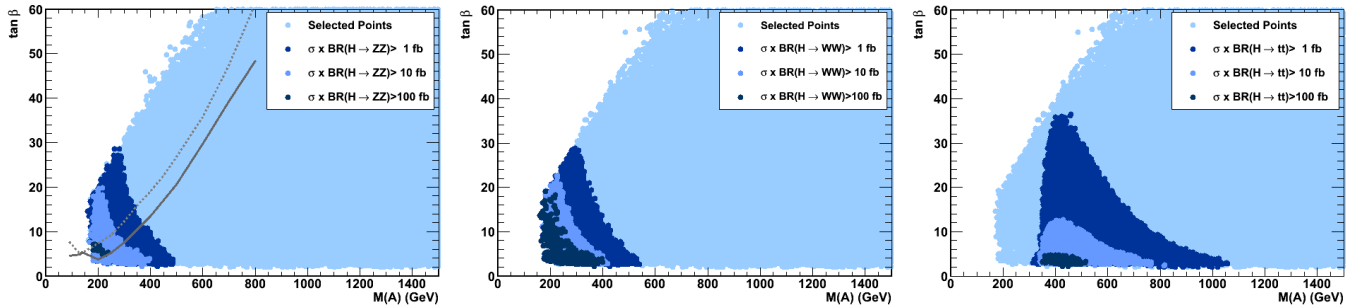


FIG. 10: Product of production cross section and decay branching fraction for $H \rightarrow ZZ$ (left), $H \rightarrow WW$ (upper centre) and $H \rightarrow t\bar{t}$ (right) at 8 TeV in the $[M_A - \tan\beta]$ parameter plane. The dots in the light colour show all the selected pMSSM points and those in darker shades of colour the points having $\sigma \times \text{BR}$ larger than 1, 10 and 100 fb. The lines superimposed on the left panel show the expected (dashed) and observed (continuous) 95% C.L. upper limits obtained in the $H/A \rightarrow \tau\tau$ search of [51]. Entries below threshold in the $t\bar{t}$ channel are due to off-shell decays.

sensitivity corresponds to an expected upper limit on the product of production cross section and decay branching fraction of ~ 80 fb at 300 GeV and 20 fb at 500 GeV. In this study, we impose the expected CMS 95% C.L. limit on the product of production cross section and decay branching fraction, which is weaker than the observed limit, on our pMSSM points.

The production and decay pattern of the heavy MSSM neutral Higgs bosons crucially depend on the value of $\tan\beta$, as discussed above. The LHC data at 7 and 8 TeV, probe relatively large values, $\tan\beta \gtrsim 5-10$. For these values, their couplings to b quarks and τ leptons, proportional to $\tan\beta$, are strongly enhanced, and those to top quarks and massive bosons, proportional to $\approx 1/\tan\beta$, are suppressed. Therefore the $\tau\tau$ channel is presently the single most constraining decay mode. It defines a region of the $[M_A - \tan\beta]$ parameter space which is probed also by the $B_s \rightarrow \mu\mu$ rare decay and by dark matter direct detection experiments [14, 15], but the $H/A \rightarrow \tau\tau$ LHC searches at 7 and 8 TeV set the tightest constraints. In addition to it, preliminary results have been reported for the first search for $H/A \rightarrow b\bar{b}$ in associate production with b jets $bbH/A \rightarrow bbbb$ based on the 7 TeV CMS data [52], which has sensitivity at large values of $\tan\beta$ with an expected upper limit of 8 pb on $\sigma \times \text{BR}$ at 300 GeV. The analyses of the decays of the SM Higgs $H_{SM} \rightarrow ZZ$ have set constraints on the product of production cross section and decay branching fraction $\sigma(gg \rightarrow H_{SM}) \times \text{BR}(H_{SM} \rightarrow ZZ)$ for Higgs masses up to 1 TeV [53, 54]. These can now be used to constrain the decay of the heavy SUSY $H/A \rightarrow ZZ$, with upper limits of ~ 1.9 and 1.4 fb at 200 and 300 GeV, respectively. Finally, the decay $H/A \rightarrow t\bar{t}$ can be constrained through the cross section bounds obtained for the production of a narrow resonance decaying into top quark pairs, interpreted in the original studies in the context of the searches for the production of a lepto-phobic Z' gauge boson, KK resonances or other exotic narrow resonances. Results have been reported by both ATLAS [55] and CMS [56] for the 7 TeV data with cross section upper limits of order of 3 pb and 0.8 pb at resonance masses of

~ 500 GeV and 800 GeV, respectively.

First, we study the value of the product of production cross section and decay branching fraction in several channels by scanning over the pMSSM parameters. Figure 10 shows the regions of the $[M_A - \tan\beta]$ parameter space where the product $\sigma \times \text{BR}$ exceeds 1, 10 and 100 fb at 8 TeV for the $gg \rightarrow H/A$ and $bb \rightarrow H/A$ production processes and the $H/A \rightarrow ZZ$, $H/A \rightarrow WW$ and $H/A \rightarrow t\bar{t}$ decays. Finally, we combine the constraints derived in the various channels. We take the expected upper limits on the products $\sigma \times \text{BR}$ in the various channels for both (a) the present status of the results and (b) their extrapolation to the full 8 TeV data set of 25 fb^{-1} . When limits are only available for the 7 TeV data set, we compute the expected limit at 8 TeV by taking the ratio of production cross sections at the two energies, as a function of the H/A mass, into account. For each channel, we consider the contours in the $[M_A - \tan\beta]$ plane where more than 95% of the selected pMSSM points are excluded by these constraints. Alongside the $\tau\tau$ channel, the ZZ and $bbbb$ channels also offer sensitivity on the 7 and 8 TeV data. For the ZZ channel we use the upper limits on $\sigma \times \text{BR}$ from [54]. These limits define an excluded region which connects with the $\tau\tau$ constraint at low masses and extends up to $M_A \simeq 550$ GeV for $\tan\beta = 3-4$. The $bbbb$ channels is based on the preliminary result on the 7 TeV CMS data [52] extrapolated to the full 8 TeV data set. We include also the constraint derived from the signal strengths, μ , obtained in the ATLAS and CMS SM Higgs analyses for the $\gamma\gamma$, WW , ZZ channels and the limits for bb and $\tau\tau$, as discussed above, interpreting the observed particle as the SUSY lightest Higgs, h . Results are summarised in Figure 11. The combination of the $H/A \rightarrow \tau\tau$ channel and the mass and μ values for the lightest h boson exclude the region with $M_A > 320$ GeV for all values of $\tan\beta$. For the current results, the μ values defines this lower bound in the region of $\tan\beta = 2-15$, where the direct search sensitivity is weaker. The sensitivity of the direct H/A searches should approach this bound down to $\tan\beta \simeq 10$, once the full 2012 data is analysed. The

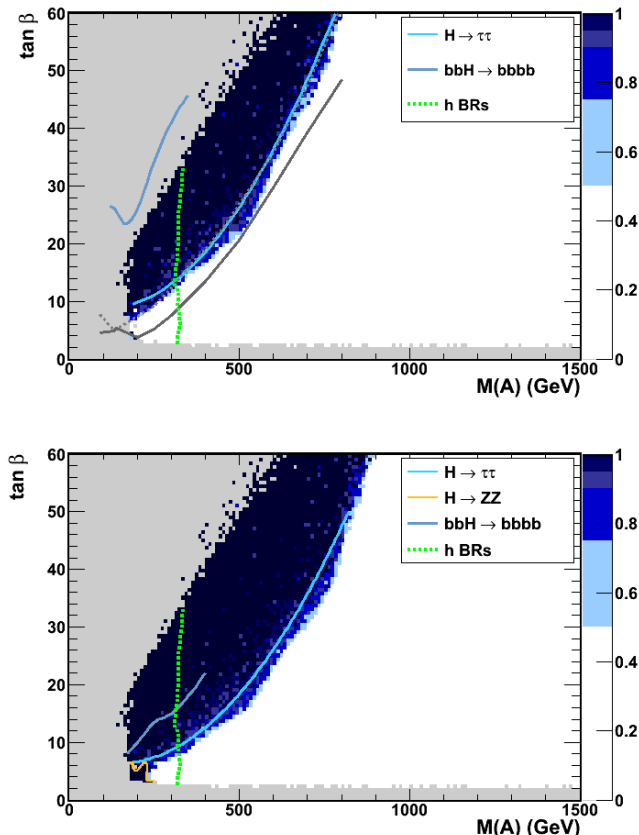


FIG. 11: Combination of the expected constraints on the $[M_A - \tan\beta]$ parameter plane from the $\tau\tau$ and ZZ channels for (a) the current results (upper panel) and (b) their extrapolation to the full 8 TeV data set (lower panel). The colour scale gives the fraction of pMSSM points excluded at each M_A and $\tan\beta$ value. The contours show the limits corresponding to 95% or more of the points excluded. The 90% C.L. constraint from the Higgs signal strengths is also shown. The expected and observed upper limits on $\tan\beta$ obtained in the MSSM M_h^{max} scenario from the $\tau\tau$ channel search of [51] are indicated by the grey dotted and continuous lines, respectively, on the upper plot. The grey region has no accepted pMSSM points after the $B_s \rightarrow \mu\mu$, direct DM searches and M_h constraints.

ZZ channel, and to a lesser extent the WW , should close the low M_A corner from $\tan\beta \simeq 2$ up to the $\tau\tau$ limit for $M_A \lesssim 230$ GeV with the full 8 TeV data. The upper limits from the $t\bar{t}$ channel, for which only results at 7 TeV have been reported, are still below the expected values for H/A production in the MSSM, even by extrapolating them to the full 8 TeV data set. Instead, this channel will become essential at 13 and 14 TeV. The combination of these constraints from the Higgs sector provide limits on M_A and $\tan\beta$, which are significantly tighter compared to those derived from flavour physics, such as the $\text{BR}(B_s \rightarrow \mu\mu)$ for which the first measurement has recently been reported by LHCb [16] (see Figure 11).

B. Perspectives at 14 TeV

The increase of the production cross sections moving from 7 to 14 TeV is a factor of 4.5 to 9 for $gg \rightarrow H/A$ and 5 to 12 for $bb \rightarrow H/A$ in the mass range 300 to 800 GeV. Figure 12 shows the regions of the $[M_A - \tan\beta]$ parameter space where the product $\sigma \times \text{BR}$ exceeds 1, 10 and 100 fb for the $gg \rightarrow H/A$ and $bb \rightarrow H/A$ production processes and the $H/A \rightarrow ZZ$, $H/A \rightarrow WW$, $H/A \rightarrow hh$, $A \rightarrow hZ$, $H/A \rightarrow t\bar{t}$ and the inclusive decays $H/A \rightarrow \text{SUSY}$ particles. At the high mass end the product $\sigma \times \text{BR}$ of ~ 10 fb, corresponding to the current sensitivity at 800 GeV in the $\tau\tau$ channel, is obtained beyond $M_A = 1$ TeV. At 13 and 14 TeV the sensitivity extends to mass values above the hh , hZ and the tt production thresholds at small to intermediate values of $\tan\beta$, which make these channels relevant to the LHC searches. In this region the $\tau\tau$ channel alone cannot ensure the coverage of the $[M_A - \tan\beta]$ plane and these additional channels need to be included. The ZZ channel provides redundancy while the tt decay is most important, in particular at large M_A and low $\tan\beta$ values. The WW channel has more limited interest, since its sensitivity is lower than ZZ . The combination of the $\tau\tau$, ZZ and tt modes covers the $[M_A - \tan\beta]$ parameter plane up to $M_A \simeq 700$ GeV for any value of $\tan\beta$, as shown in Figure 13.

1. Characterisation of hZ and hh channels

The decays $H \rightarrow hh$ and $A \rightarrow hZ$ are important in providing redundancy at low values of $\tan\beta$ and intermediate M_A masses. They also result in rather distinctive $bbbb$, $bb\tau\tau$ and $bb\ell\ell$ ($\ell = e, \mu$) final states, which should be investigated in the high energy LHC runs. Since these modes have not yet been searched for in the LHC data, we characterise here their decay kinematics and study the reconstruction strategies using a simple analysis for signal events.

These events are generated using Pythia 8.1 [57] at 14 TeV and scaled to an integrated luminosity of 150 fb^{-1} . For this study, we have chosen $M_A = 400$ and 500 GeV, $\tan\beta = 5$ with branching fractions of 0.12 for $H \rightarrow hh$ and $A \rightarrow hZ$. The detector response simulation is performed using Delphes 3.0 [58]. Jets are reconstructed using the anti-kt algorithm [59] implemented in FastJet [60], requiring their pseudo-rapidity, η , not to exceed 2.8 and transverse momentum $p_T > 20$ GeV. Electrons and muons are accepted for $|\eta| < 2.4$ and $p_T > 20$ GeV. b -jets are accepted at $\eta < 2.5$, assuming a tagging efficiency of 75% per jet. In both channels, b jets are rather soft, with the transverse energy distributions peaking around 50 GeV, thus emphasising b tagging at relatively small transverse energies (see Figures 14 and 15). Similarly low is the transverse energy distribution of leptons from the Z decay in the A channel, which has its most probable value just above the p_T cut applied in this analysis (see Figure 15).

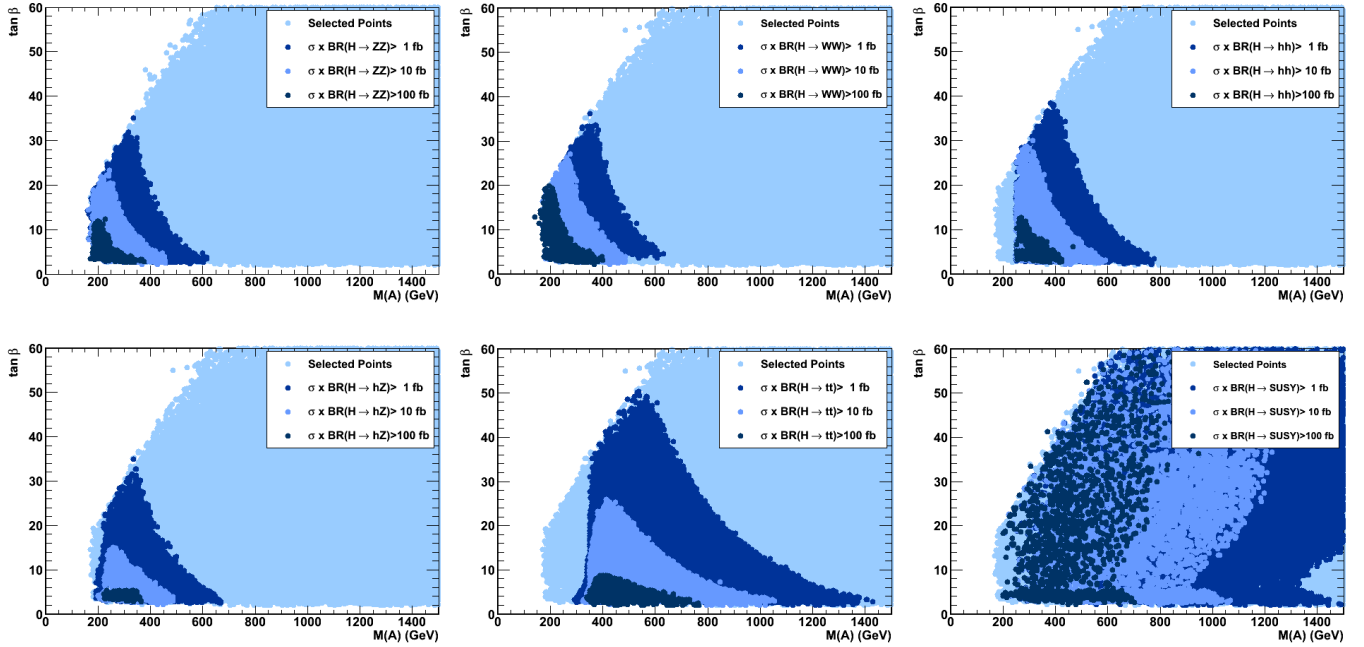


FIG. 12: Product of production cross section and decay branching fraction for $H \rightarrow ZZ$ (upper left), $H \rightarrow WW$ (upper centre), $H \rightarrow hh$ (upper left), $A \rightarrow hZ$ (bottom right), $H \rightarrow t\bar{t}$ (bottom centre) and $H \rightarrow$ SUSY particles (bottom left), at 14 TeV in the $[M_A - \tan\beta]$ parameter plane. The colour coding is given in the legend and it is the same as in Figure 10.

$H \rightarrow hh \rightarrow bbbb$ events are reconstructed by requiring at least three b -tagged jets. The pairing of four b jets, or three b jets with any of the reconstructed jets, which minimises the mass difference of the two di-jet pairs and their difference from the h mass of 126 GeV is selected. The di-jet invariant mass distribution is shown in Figure 14. The invariant mass resolution obtained with the fast simulation is comparable to that reported for the $H_{SM} \rightarrow b\bar{b}$ search. The four-jet invariant mass, M_{bbbb} shows a clear peak corresponding to the generated H mass as shown in

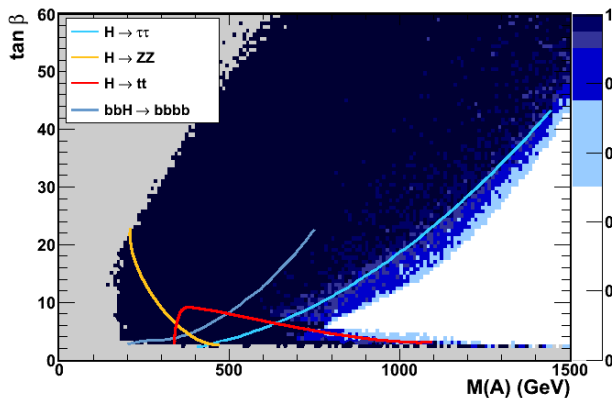


FIG. 13: Combination of the expected constraints on the $[M_A - \tan\beta]$ parameter plane from the $\tau\tau$, ZZ and tt channels as in Figure 11, extrapolated to 150 fb^{-1} at 14 TeV. The colour scale gives the fraction of pMSSM points excluded at each M_A and $\tan\beta$ value. The grey region has no accepted pMSSM points after the $B_s \rightarrow \mu\mu$, direct DM searches and M_h constraints.

Figure 14. The efficiency of this selection for the signal mass region of $300 < M_{bbbb} < 500$ GeV is $\simeq 16\%$ at both values of M_H .

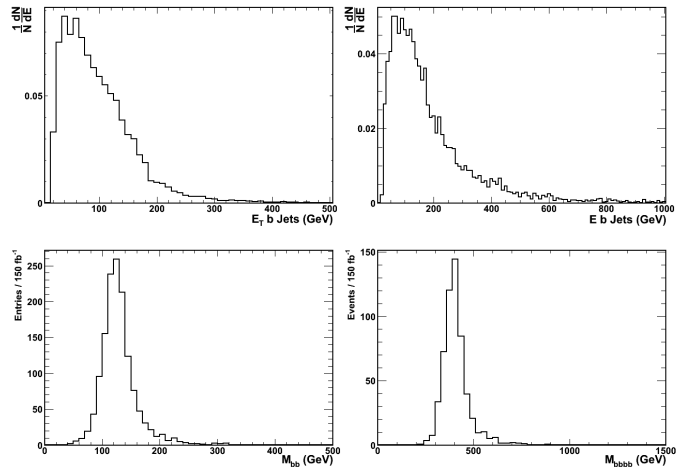


FIG. 14: Reconstruction of $H \rightarrow hh \rightarrow bbbb$ events at 14 TeV for $M_H = 400$ GeV: distribution of the b -jet transverse energy E_T (upper right) and energy E (lower left), invariant mass of bb pairs (lower left) and $bbbb$ invariant mass (lower right). A $\text{BR}(H \rightarrow hh) = 0.12$ has been assumed.

For the $Zh \rightarrow \ell\ell bb$ we select events with two, oppositely charged, electrons or muons with two or more jets, of which at least one b tagged. The $\ell\ell$ invariant mass is required to be consistent with that of the Z within the resolution. If the event contains exactly two b -tagged jets, the invariant mass of the pair is required to be con-

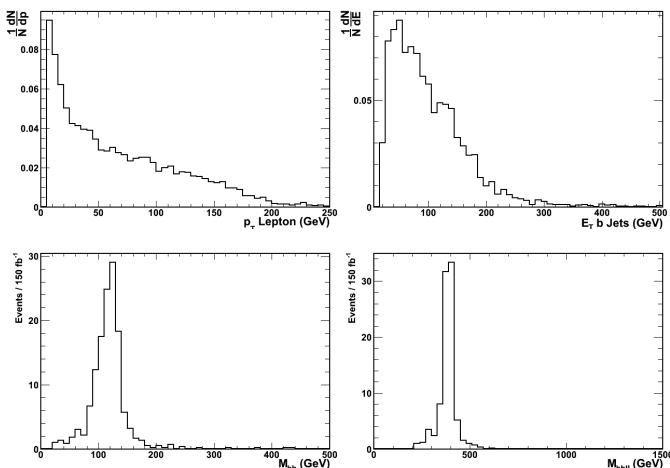


FIG. 15: Reconstruction of $A \rightarrow Zh \rightarrow \ell\ell b\bar{b}$ events at 14 TeV for $M_A = 400$ GeV: distribution of the lepton transverse energy p_T (upper left), b -jet transverse energy E_T (upper right), $b\bar{b}$ (lower left) and $b\bar{b}l\bar{l}$ (lower right) invariant mass. A $\text{BR}(A \rightarrow Zh) = 0.12$ has been assumed.

sistent with 126 GeV within the resolution. If there is only one b -tagged jet, but it has a mass consistent with 126 GeV, this is also accepted. The final mass is computed by combining the di-leptons with the di-jet pair or the single b jet. The resulting distribution is shown in Figure 15 for an integrated luminosity of 150 fb^{-1} . The selection efficiency for the loose signal mass region of $300 < M_{b\bar{b}l\bar{l}} < 500$ GeV is $\simeq 25\%$ at both values of M_A .

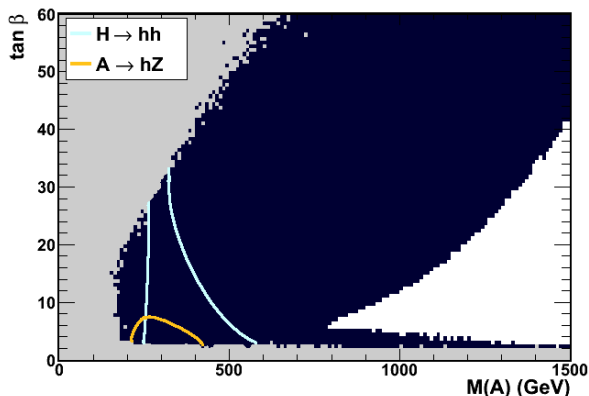


FIG. 16: Regions on the $[M_A - \tan\beta]$ parameter plane where the $H \rightarrow hh$ and $A \rightarrow hZ$ process yield 50 reconstructed events for 150 fb^{-1} at 14 TeV, compared with the coverage provided by the combination of $\tau\tau$ and ZZ shown in dark blue. The grey region has no accepted pMSSM points after the $B_s \rightarrow \mu\mu$, direct DM searches and M_h constraints.

Since we base this preliminary characterisation on the reconstruction of signal only event and have not considered the backgrounds, we cannot define here exclusion contours. Instead, we simply plot the regions of the $[M_A - \tan\beta]$ plane where we register more than 50 reconstructed events for 150 fb^{-1} of data at 14 TeV. The result is shown in Figure 16, where the region covered by the

hh and hZ final states is compared to that of expected sensitivity for the combination of the $\tau\tau$, ZZ and $t\bar{t}$ channels, considered above. We notice that the hh channel covers the full $\tan\beta$ range of interest from threshold up to $M_A \simeq 400$ GeV and up to 550 GeV at low $\tan\beta$ values, beyond the ZZ sensitivity. In this important region of small to intermediate values of $\tan\beta$, the hh and hZ channels provide redundancy to the coverage offered by the $\tau\tau$ and $t\bar{t}$ modes.

C. Effect of QCD Uncertainties and SUSY Particles

The limits derived above do not account for the effects of theoretical uncertainties, affecting the Higgs production cross section and decay branching fractions, and of SUSY contributions. First, the $gg \rightarrow H/A$ and $b\bar{b} \rightarrow H/A$ cross sections have sizeable QCD uncertainties from the factorisation and renormalisation scales, parton distribution functions (PDFs) and parametric systematics from α_s and the heavy quark masses. We estimate the parametric systematics on the cross section for $\alpha_s = 0.118 \pm 0.0012$, $\bar{m}_b(\bar{m}_b) = (4.19 \pm 0.05)$ GeV, $m_t = (172.9 \pm 1.5)$ GeV and those from the PDFs by taking the largest difference between different sets of functions. The latter is the dominant contribution. The combination of the uncertainties on the quark masses, PDFs and α_s leads to an estimated systematic uncertainty on the $pp \rightarrow H/A$ rate of $\approx \pm 24\%$ at 8 TeV and $\approx \pm 20\%$ at 14 TeV, dominated by the PDFs and scale, and comparable to those for $pp \rightarrow H_{\text{SM}}$ production [61, 62].

In order to evaluate their impact on the exclusion contours in the $[M_A - \tan\beta]$ plane, we repeat our study while changing the production cross section by $\pm 25\%$ and compare the constraints obtained to that corresponding to the central values for the production cross sections. Figures 17 and 18 show the fractions of excluded points in the $[M_A - \tan\beta]$ plane and their projections as a function of M_A for the fixed value of $\tan\beta = 15$ at 8 and 14 TeV, respectively, and includes the effect of the $\pm\sigma_{\text{QCD}}$ change of the cross sections by the QCD uncertainties. The effect is a shift of the excluded M_A mass by ± 45 GeV at 8 TeV and by ± 55 GeV at 14 TeV at $\tan\beta=15$ and larger for higher values of $\tan\beta$.

Then, we observe that, there is a significant smearing of the curve giving the fraction of excluded pMSSM points as a function of M_A , even if the systematics on the production cross section are ignored. In fact, the exclusion curve goes from 10% to 90% of the points excluded over a range of M_A values spanning ~ 90 GeV at 8 TeV and ~ 150 GeV at 14 TeV, as a result of the variation of other pMSSM parameters. This range, which is comparable to that corresponding to the QCD uncertainty obtained above, is intrinsic to the pMSSM and includes contributions such as the loop effect through the Δ_b term discussed in section II.B.

Finally, we consider quantitatively the region of the

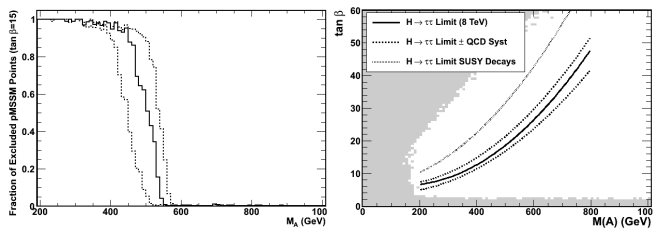


FIG. 17: QCD systematics and SUSY particle effects on the projected $H/A \rightarrow \tau\tau$ exclusion with at 8 TeV. Left: fraction of pMSSM points excluded for $\tan\beta = 15$ as a function of M_A (continuous line) and the effect of a change by $\pm 25\%$ of the $pp \rightarrow H/A$ production cross section to reflect QCD uncertainties (dashed lines). Right: limits from the $\tau\tau$ in the $[M_A - \tan\beta]$ plane obtained by varying the production cross section (dashed lines) and requiring less than 0.1% of the points around the limit to fail exclusion due to the effect of SUSY decays. The grey region has no accepted pMSSM points after the $B_s \rightarrow \mu\mu$, direct DM searches and M_h constraints.

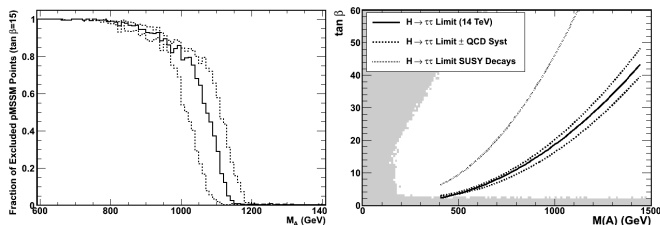


FIG. 18: QCD systematics and SUSY particle effects on the projected $H/A \rightarrow \tau\tau$ exclusion, as in Figure 17, for 150 fb^{-1} at 14 TeV.

$[M_A - \tan\beta]$ plane where decays into SUSY channels may invalidate the $\tau\tau$ limit. The panels on the right in Figures 17 and 18, have dashed lines showing the limit of the region where this may occur, for 8 and 14 TeV, respectively. Since the $\sigma \times \text{BR}(H/A \rightarrow \tau\tau)$ product increases for low M_A and high $\tan\beta$ values, there is a region where the SUSY decays cannot upset the exclusion obtained in this channel, since the $H \rightarrow \text{SUSY}$ branching fraction is $\lesssim 0.60$, as shown in Figure 4. However, the region affected by the SUSY decays extends much further towards lower A masses compared to that describing the effect of the QCD and parametric uncertainties on the production cross section and also the SUSY loop effects. The width of this region, $\sim 150 \text{ GeV}$ at 8 TeV for $\tan\beta = 15$, and the occurrence of these points increase with the energy which gives access to heavier bosons with decays into pairs of SUSY particles kinematically allowed. Moving from 8 to 14 TeV, the width of the regions doubles and the occurrence of these points increase by a factor of ~ 1.5 . The occurrence of the various SUSY effects we have discussed for the pMSSM points within the region of the $[M_A - \tan\beta]$ plane excluded in the MSSM M_h^{max} model but not excluded due to their low value of the $\sigma \times \text{BR}(H/A \rightarrow \tau\tau)$ product has been studied for our scans. We observe that H/A decays into $\tilde{\chi}\tilde{\chi}$ pairs are responsible for 55% of the

cases and those into $\tilde{\tau}\tilde{\tau}$ pairs for another 10%, while it is a Δ_b term large and negative in sign which suppresses the $\tau\tau$ rate for the remaining 35% of the points failing exclusion. When the H decays into $\tilde{\chi}\tilde{\chi}$ pair, the dominant state is the lightest neutralino $\tilde{\chi}_1^0$ in about 1/4 of the cases. In the other cases, we observe an increase in the yield of $\tilde{\chi}_{2,3}^0 \rightarrow h/Z\tilde{\chi}_1^0$, which may offer an important signature for the LHC searches [63].

IV. CONCLUSIONS

The search for heavy Higgs bosons represents a next frontier in the understanding of the Higgs sector after the discovery of the Higgs-like state at 126 GeV at the LHC and the first results on its decays, spin and parity. The combination of the indirect limits from the h signal strengths and the direct searches in the $\tau\tau$ and ZZ channels should impose an exclusion limits in $[M_A - \tan\beta]$ plane around $M_A \gtrsim 320 \text{ GeV}$ for the 7+8 TeV data, determined by the indirect limit from the rates of the observed Higgs boson

As the mass sensitivity of the LHC searches increases with the energy and integrated luminosity, more final states than $\tau\tau$ become relevant to effectively constrain the supersymmetric parameter space, in particular at low to moderate values of $\tan\beta$. In fact, low values of $\tan\beta$ are still viable, after incorporating the M_h constraint, provided high SUSY scales, M_S , are chosen and they represent a scenario, rich in decays into $t\bar{t}$ and ZZ , hh and hZ boson pairs, which should be carefully explored at the LHC at 13 and 14 TeV. The M_S bound will reach $M_A \gtrsim 800 \text{ GeV}$ for any value of $\tan\beta$ with 150 fb^{-1} of data at 14 TeV, determined by the direct searches for heavy Higgs states. The effects of the SUSY particle spectrum, other SUSY parameters and the QCD theoretical uncertainties need to be carefully considered. SUSY loops and QCD effects on the M_A bounds are found to be quite comparable in size. However, scenarios where decays into SUSY particles are important, or even dominant, exist and these channels need to be accounted for in the LHC searches at 13 and 14 TeV.

The constraints derived by the study of the Higgs sector are becoming an essential part of the probe of the SUSY parameter space at the LHC and offer an essential complement to the searches for strongly interacting SUSY particles and gauginos.

Acknowledgments

We are grateful to Abdelhak Djouadi who provided us with inspiration for several parts of this study, in particular the interest for the low $\tan\beta$ region and the use of the ZZ and $t\bar{t}$ analyses to constrain heavy Higgs production. We wish to thank also Benjamin Allanach for discussion and support with the use of Softsusy, Robert Harlander with that of SusHi and Stefan Dittmaier for discus-

sion on the QCD systematics in Higgs production. M.B. wishes to thank the Galileo Galilei Institute for Theo-

retical Physics for the hospitality and INFN for partial support during the early stages of this work.

-
- [1] G. Aad *et al.* [ATLAS Collaboration], Phys. Lett. B **716** (2012) 1 [arXiv:1207.7214 [hep-ex]].
- [2] S. Chatrchyan *et al.* [CMS Collaboration], Phys. Lett. B **716** (2012) 30 [arXiv:1207.7235 [hep-ex]].
- [3] J. Baglio and A. Djouadi, arXiv:1103.6247 [hep-ph].
- [4] M. Carena, P. Draper, T. Liu and C. Wagner, Phys. Rev. D **84** (2011) 095010 [arXiv:1107.4354 [hep-ph]].
- [5] N. D. Christensen, T. Han and S. Su, Phys. Rev. D **85** (2012) 115018 [arXiv:1203.3207 [hep-ph]].
- [6] J. Chang, K. Cheung, P. -Y. Tseng and T. -C. Yuan, Phys. Rev. D **87** (2013) 035008 [arXiv:1211.3849 [hep-ph]].
- [7] M. Carena, S. Heinemeyer, O. Stal, C. E. M. Wagner and G. Weiglein, arXiv:1302.7033 [hep-ph].
- [8] A. Djouadi *et al.* [Les Houches MSSM Working Group], hep-ph/9901246.
- [9] [ATLAS Collaboration], CERN/LHCC 99-14.
- [10] A. Djouadi, Phys. Rept. **459** (2008) 1 [hep-ph/0503173].
- [11] M. Muhlleitner, H. Rzehak and M. Spira, DESY-PROC-2010-01.
- [12] A. Arbey, M. Battaglia, A. Djouadi and F. Mahmoudi, JHEP **1209** (2012) 107 [arXiv:1207.1348 [hep-ph]].
- [13] A. Arbey, M. Battaglia, A. Djouadi and F. Mahmoudi, Phys. Lett. B **720** (2013) 153 [arXiv:1211.4004 [hep-ph]].
- [14] A. Arbey, M. Battaglia and F. Mahmoudi, Eur. Phys. J. C **72** (2012) 1906 [arXiv:1112.3032 [hep-ph]].
- [15] A. Arbey, M. Battaglia, F. Mahmoudi and D. Martinez Santos, Phys. Rev. D **87** (2013) 035026 [arXiv:1212.4887 [hep-ph]].
- [16] R. Aaij *et al.* [LHCb Collaboration], Phys. Rev. Lett. **110** (2013) 021801 [arXiv:1211.2674 [hep-ex]].
- [17] E. Aprile *et al.* [XENON100 Collaboration], Phys. Rev. Lett. **109** (2012) 181301.
- [18] A. Arbey, M. Battaglia and F. Mahmoudi, Eur. Phys. J. C **72** (2012) 1847 [arXiv:1110.3726 [hep-ph]].
- [19] A. Djouadi, J. Kalinowski and M. Spira, Comput. Phys. Commun. **108** (1998) 56.
- [20] M. Spira, A. Djouadi, D. Graudenz and P. M. Zerwas, Nucl. Phys. B **453** (1995) 17 [hep-ph/9504378].
- [21] M. Spira, Nucl. Instrum. Meth. A **389** (1997) 357 [hep-ph/9610350].
- [22] R.V. Harlander and W.B. Kilgore, Phys. Rev. D **68** (2003) 013001 [hep-ph/0304035].
- [23] M. Spira, Fortsch. Phys. **46** (1998) 203 [hep-ph/9705337].
- [24] R. V. Harlander, S. Liebler and H. Mantler, arXiv:1212.3249 [hep-ph].
- [25] B.C. Allanach, Comput. Phys. Commun. **143** (2002) 305 [arXiv:hep-ph/0104145 [hep-ph]].
- [26] F. Mahmoudi, Comput. Phys. Commun. **178** (2008) 745 [arXiv:0710.2067 [hep-ph]]; *idem*, Comput. Phys. Commun. **180** (2009) 1579 [arXiv:0808.3144 [hep-ph]].
- [27] A. Arbey and F. Mahmoudi, Comput. Phys. Commun. **181** (2010) 1277 [arXiv:0906.0369 [hep-ph]].
- [28] D. M. Pierce, J. A. Bagger, K. T. Matchev, R. -j. Zhang and , Nucl. Phys. B **491** (1997) 3 [hep-ph/9606211].
- [29] W. Hollik and J. -H. Zhang, Phys. Rev. D **84** (2011) 055022 [arXiv:1109.4781 [hep-ph]].
- [30] P. Gonzalez, S. Palmer, M. Wiebusch and K. Williams, arXiv:1211.3079 [hep-ph].
- [31] R. Barate *et al.* [ALEPH, DELPHI, L3 and OPAL Collaborations and LEP Working Group for Higgs boson searches], Phys. Lett. B **565** (2003) 61 [hep-ex/0306033].
- [32] S. Schael *et al.* [ALEPH, DELPHI, L3 and OPAL Collaborations and LEP Working Group for Higgs Boson Searches], Eur. Phys. J. C **47** (2006) 547 [hep-ex/0602042].
- [33] M. S. Carena, S. Heinemeyer, C. E. M. Wagner, G. Weiglein and , Eur. Phys. J. C **26** (2003) 601 [hep-ph/0202167].
- [34] R. D. Ball, M. Bonvini, S. Forte, S. Marzani and G. Ridolfi, arXiv:1303.3590 [hep-ph].
- [35] [ATLAS Collaboration], Note ATLAS-CONF-2013-012.
- [36] [CMS Collaboration], Note CMS PAS HIG-2013-001.
- [37] [ATLAS Collaboration], Note ATLAS-CONF-2013-013.
- [38] [CMS Collaboration], Note CMS PAS HIG-2013-002.
- [39] [ATLAS Collaboration], Note ATLAS-CONF-2013-030.
- [40] [CMS Collaboration], Note CMS PAS HIG-2013-003.
- [41] [CMS Collaboration], Note CMS PAS HIG-2013-004.
- [42] J. Beringer *et al.* [Particle Data Group Collaboration], Phys. Rev. D **86** (2012) 010001.
- [43] [ATLAS Collaboration], Note ATLAS-CONF-2012-161.
- [44] [CMS Collaboration], Note CMS PAS HIG-2012-044.
- [45] T. Aaltonen *et al.* [CDF and D0 Collaborations], Phys. Rev. Lett. **109** (2012) 071804 [arXiv:1207.6436 [hep-ex]].
- [46] [ATLAS Collaboration], Note ATLAS-CONF-2013-014.
- [47] [ATLAS Collaboration], Note ATLAS-CONF-2012-161.
- [48] M. Schmelling, Phys. Scripta **51** (1995) 676.
- [49] P. Bechtle, S. Heinemeyer, O. Stal, T. Stefaniak, G. Weiglein and L. Zeune, arXiv:1211.1955 [hep-ph].
- [50] G. Aad *et al.* [ATLAS Collaboration], Phys. Lett. B **705** (2011) 174 [arXiv:1107.5003 [hep-ex]].
- [51] [CMS Collaboration], Note CMS PAS HIG-2012-050.
- [52] J. Behr *et al.* arXiv:1301.4412 [hep-ex].
- [53] [ATLAS Collaboration], Note ATLAS-CONF-2012-169.
- [54] [CMS Collaboration], Note CMS PAS HIG-2012-041.
- [55] G. Aad *et al.* [ATLAS Collaboration], JHEP **1209** (2012) 041 [arXiv:1207.2409 [hep-ex]].
- [56] S. Chatrchyan *et al.* [CMS Collaboration], arXiv:1211.3338 [hep-ex].
- [57] T. Sjöstrand, S. Mrenna and P. Skands, JHEP **05** (2006) 026; *eadem*, Comput. Phys. Commun. **178** (2008) 852.
- [58] S. Oryn, X. Rouby and V. Lemaitre, arXiv:0903.2225 [hep-ph].
- [59] M. Cacciari, G.P. Salam and G. Soyez, JHEP **04** (2008) 063 [arXiv:0802.1189 [hep-ph]].
- [60] M. Cacciari, G.P. Salam and G. Soyez, Eur. Phys. J. C **72** (2012) 1896 [arXiv:1111.6097 [hep-ph]]; *eadem*, Phys. Lett. B **641** (2006) 57 [hep-ph/0512210].
- [61] S. Dittmaier, C. Mariotti, G. Passarino, and R. Tanaka (Eds.) [LHC Higgs Cross Section Working Group], CERN-2011-002, arXiv:1101.0593 [hep-ph].
- [62] S. Dittmaier, C. Mariotti, G. Passarino, and R. Tanaka (Eds.) [LHC Higgs Cross Section Working Group], CERN-2012-002, arXiv:1201.3084 [hep-ph].

- [63] A. Arbey, M. Battaglia and F. Mahmoudi, arXiv:1212.6865 [hep-ph].